Chinese Journal of Aeronautics, (2013),26(6): 1439–1448

Chinese Society of Aeronautics and Astronautics
& Beihang University

Chinese Journal of Aeronautics

cja@buaa.edu.cn
www.sciencedirect.com

Flight dynamics modeling of a small ducted fan aerial vehicle based on parameter identification

Wang Zhengjie [a,*], Liu Zhijun [a], Fan Ningjun [a], Guo Meifang [b]

[a] *School of Mechatronical Engineering, Beijing Institute of Technology, Beijing 100081, China*
[b] *North Institute for Science & Technical Information, Beijing 100089, China*

Received 10 March 2013; revised 10 May 2013; accepted 30 August 2013
Available online 6 November 2013

KEYWORDS

Aerodynamics;
Experimental aerodynamics;
Flight vehicle design;
Multidisciplinary design optimization;
Structural design

Abstract This paper presents a simple and useful modeling method to acquire a dynamics model of an aerial vehicle containing unknown parameters using mechanism modeling, and then to design different identification experiments to identify the parameters based on the sources and features of its unknown parameters. Based on the mathematical model of the aerial vehicle acquired by modeling and identification, a design for the structural parameters of the attitude control system is carried out, and the results of the attitude control flaps are verified by simulation experiments and flight tests of the aerial vehicle. Results of the mathematical simulation and flight tests show that the mathematical model acquired using parameter identification is comparatively accurate and of clear mechanics, and can be used as the reference and basis for the structural design.

1. Introduction

The ducted fan aerial vehicle is a new kind of single-blade rotor aircraft which is different from traditional fixed-wing craft and helicopters. This new kind of aerial vehicle has more compact architecture and the attitude controls can deal with more complex flow patterns. From the beginning of the 1990s, many countries have started research in this field one after another, and have developed different ducted aerial vehicles.[1,2] Single-blade ducted aerial vehicles have shown great potential in the military field and humanitarian relief. In recent years, related research institutions have continuously invested money in technology research in different fields, among which aerodynamic configuration design, airframe structure design, testing methods and control methods have become the important fields.[3–6]

Ducted fan aerial vehicles are unstable static system. Good controllability is a precondition for the stable flight of an aerial vehicle, and the controllability of the aerial vehicle is closely related to the structural parameters of the vehicle. The precondition for realizing a stable flight is to find proper controllability conditions for the miniature aerial vehicles, and based on those conditions to carry out a structural design for the aerial vehicle. Therefore, it is crucial to find a modeling method which can reflect the features of the internal structure of the vehicle and has comparatively accurate model parameters.

There are two ways to construct a mathematical model for a system. One is mechanism modeling and the other is system identification modeling. Mechanism modeling can produce a mathematical model for a ducted aerial vehicle. Based on this

* Corresponding author. Tel.: +86 10 68914332.
E-mail address: wangzhengjie@bit.edu.cn (Z. Wang).

Peer review under responsibility of Editorial Committee of CJA.

ELSEVIER Production and hosting by Elsevier

http://dx.doi.org/10.1016/j.cja.2013.10.006

traditional methods, Marconi, et al.[7] studied a simple ducted fan micro air vehicle (MAV) based on a single fixed pitch rotor and four active aerodynamic surfaces and investigated the dynamical model of this MAV. Naldi, et al.[8] provided a nonlinear dynamical model of the system which is able to describe stationary flight, fast forward flight and the transitions between the two flight conditions. Ko, et al.[9] obtained the model of the ducted fan vehicles by a kind of modeling software tool that has been validated through various wind tunnel tests and flight tests of ducted fan vehicles. However, as the architecture of such an aerial vehicle is special, the parameters of the model cannot be obtained accurately using analysis. Using the actual input and output data of the aerial vehicle, the system identification can produce a mathematical model for the aerial vehicle. In contrast, this paper aims to present few preliminary results for acquiring the dynamics model by using experimental methods. Then, based on the obtained dynamics model, the method for the structure design of the control surfaces is carried out.

2. Flight dynamics modeling

2.1. System composition of ducted fan aerial vehicle

This kind of aerial vehicle is composed of three parts, which are the power system, the attitude control system and the airframe system, as shown in Fig. 1. The power system includes the brushless DC motor, the electronic regulator, the batteries and the ducted propeller. The attitude control system is composed of two layers of aerodynamic control flaps under the propeller. These two sets of control flaps are located within the rotational flow field produced by the propeller. The airframe system includes the ring duct, the equipment cabin and the supporting structure of the airframe. The ring duct can isolate the high-speed spinning ducted propeller from the external environment in order to provide higher security during the operation. Meanwhile, the specially designed duct has significant augmented lift effect.

2.2. Flight dynamics modeling

The ducted fan aerial vehicle is a special surface symmetry system. The origin of the coordinate frame set in this paper overlaps with the location of the gravity center of the aerial vehicle. The symmetry planes of the aerial vehicle are $x_bO_bz_b$ and $y_bO_bz_b$, which are shown in Fig. 1 Therefore, the inertia moment of the aerial vehicle is

$$I_{xy} = I_{xz} = I_{yz} = 0 \tag{1}$$

The scalar forms of the corresponding forces and moments are given, respectively, by

$$\begin{cases} F_x = m(\dot{u} + qw - rv) \\ F_y = m(\dot{v} + ru - pw) \\ F_z = m(\dot{w} + pv - qu) \end{cases} \tag{2}$$

$$\begin{cases} L = I_x\dot{p} + qr(I_z - I_y) \\ M = I_y\dot{q} + rp(I_x - I_z) \\ N = I_z\dot{r} + pq(I_y - I_x) \end{cases} \tag{3}$$

where F_x, F_y and F_z are aerodynamic forces in O_bx_b axis, O_by_b axis and O_bz_b axis respectively; L, M and N are rolling moment, pitching moment and yawing moment; u, v and w are axial velocity, lateral velocity and normal velocity; $\dot{u}$, $\dot{v}$ and $\dot{w}$ are rate of axial velocity, rate of lateral velocity and rate of normal velocity; p, q and r are roll rate, pitch rate and yaw rate; $\dot{p}$, $\dot{q}$ and $\dot{r}$ are roll, pitching and yawing angular accelerations; m is the mass.

The dynamics equation of the aerial vehicle can be rewritten in vector form, shown as

$$\boldsymbol{f}^{\mathrm{b}} = \begin{bmatrix} m(\dot{u} + qw - rv) \\ m(\dot{v} + ru - pw) \\ m(\dot{w} + pv - qu) \end{bmatrix} \tag{4}$$

$$\boldsymbol{\tau}^{\mathrm{b}} = \begin{bmatrix} I_x\dot{p} + qr(I_z - I_y) \\ I_y\dot{q} + rp(I_x - I_z) \\ I_z\dot{r} + pq(I_y - I_x) \end{bmatrix} \tag{5}$$

where $\boldsymbol{f}^{\mathrm{b}}$ and $\boldsymbol{\tau}^{\mathrm{b}}$are vectors of aerodynamic force and moment in body axes.

2.2.1. Parameterization of dynamics equation

In the case of hovering or low speed and level flight, the main forces of the ducted fan aerial vehicle include gravity, thrust and moment caused by the power system, the controlling force

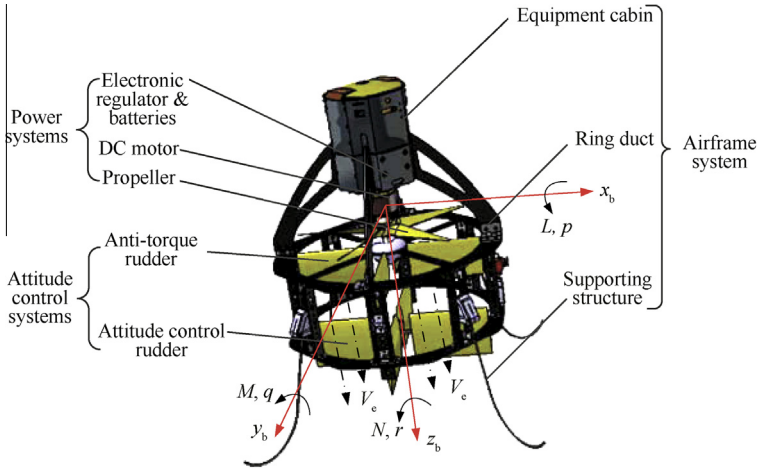

Fig. 1 Structural composition diagram.

and moment caused by the control flaps, and the spinning moment caused by a high-speed spinning propeller.[10,11] Therefore, the resultant force and moment of the aerial vehicle are given, respectively, by

$$\begin{cases} \boldsymbol{f}^{\mathrm{b}} = \boldsymbol{f}_{\mathrm{g}} + \boldsymbol{f}_{\mathrm{r}} + \boldsymbol{f}_{\mathrm{flap}} \\ \boldsymbol{\tau}^{\mathrm{b}} = \boldsymbol{\tau}_{\mathrm{r}} + \boldsymbol{\tau}_{\mathrm{flap}} + \boldsymbol{\tau}_{\mathrm{gero}} \end{cases} \tag{6}$$

where $\boldsymbol{f}_{\mathrm{g}}$, $\boldsymbol{f}_{\mathrm{r}}$ and $\boldsymbol{f}_{\mathrm{flap}}$ are gravity , thrust and control force; and $\boldsymbol{\tau}_{\mathrm{r}}$, $\boldsymbol{\tau}_{\mathrm{flap}}$ and $\boldsymbol{\tau}_{\mathrm{gero}}$ are thrust moment , control moment and spinning moment.

The explanation of the relative parameters is given below:

(1) Gravity

The gravitational force acting on the airplane acts at the center of mass (the origin point O_{b} of the body axis), and its direction is vertical downward. Because the body axis system is fixed at the center of gravity, the gravitational force will not produce any moments. Therefore, we must transform the gravitational force into its body-frame components to give:

$$\boldsymbol{f}_{\mathrm{g}} = [\, -mg\sin\theta \quad mg\cos\theta\sin\phi \quad mg\cos\theta\cos\phi \,]^{\mathrm{T}} \tag{7}$$

where θ is pitch angle, and ϕ is roll angle.

(2) Thrust and torque of the dynamic system

The thrust of the ducted fan aerial vehicle generated by the propeller has the same direction as the Oz_{b} axis. Thus the components of thrust corresponding to the Ox_{b} and Oy_{b} axes will be zero. The thrust of the dynamic system in the body axis can be written

$$\boldsymbol{f}_{\mathrm{r}} = \begin{bmatrix} 0 & 0 & -K_{\mathrm{f}}n^2 \end{bmatrix}^{\mathrm{T}} \tag{8}$$

where n is rotating speed, and aerodynamic coefficient K_{f} produced by thrust $\boldsymbol{f}_{\mathrm{r}}$ is the parameter which needs to be identified.

When the propeller spins about the Oz_{b} axis at high speed, a moment which makes the vehicle rotate about the Oz_{b} axis will be produced:

$$\boldsymbol{\tau}_{\mathrm{r}} = \begin{bmatrix} 0 & 0 & K_{\mathrm{t}}n^2 \end{bmatrix}^{\mathrm{T}} \tag{9}$$

where the aerodynamic coefficients K_{t} produced by torque $\boldsymbol{\tau}_{\mathrm{r}}$ is the parameter which needs to be identified.

(3) Aerodynamic forces and moments of the anti-torque control flaps and the attitude control flaps

Because the anti-torque control flaps use the axial symmetry system, the aerodynamic forces will only generate the resultant force corresponding with the $O_{\mathrm{b}}z_{\mathrm{b}}$ axis:

$$\boldsymbol{f}_{\mathrm{a}} = \begin{bmatrix} 0 \\ 0 \\ 4\rho S_{\mathrm{a}} V_{\mathrm{e}}^2 (C_{D\mathrm{a}}\delta_{\mathrm{a}}^2 + C_{D\mathrm{a}0}) \end{bmatrix} \tag{10}$$

where ρ the density of the air, S_{a} the effective lift area of one anti-torque flap, V_{e} the relative wind velocity generated by the propeller, $C_{D\mathrm{a}}$ the drag coefficient for a term quadratic in δ_{a}, δ_{a} the angle of the deflection of the flaps, and $C_{D\mathrm{a}0}$ the drag coefficient with zero angle of the deflection.

The aerodynamic forces formed by the reaction torque control flaps would produce a moment. This moment rotates about the Oz_{b} axis and defined by

$$\boldsymbol{\tau}_{\mathrm{a}} = \begin{bmatrix} 0 \\ 0 \\ -4\rho S_{\mathrm{a}} V_{\mathrm{e}}^2 (C_{L\mathrm{a}}\delta_{\mathrm{a}} + C_{L\mathrm{a}0}) d_{\mathrm{a}} \end{bmatrix} \tag{11}$$

where $C_{L\mathrm{a}0}$ is the lift coefficients with zero angle of the deflection, $C_{L\mathrm{a}}$ the lift coefficient considering a linear dependency of lift on the angular deflection δ_{a}, and d_{a} the distance from the location of the gravity center to the plane which is decided by the eight aerodynamic centers.

The attitude control flaps install in the interior of the ducted fan aerial vehicle, and they are positively under the reaction torque control flaps. The airfoil is the symmetry one NACA0012,[12,13] and the corresponding aerodynamic forces and moments are given by

$$\boldsymbol{f}_{\mathrm{c}} = \begin{bmatrix} \rho S_{\mathrm{c}} V_{\mathrm{e}}^2 C_{L\mathrm{c}}\delta_{\mathrm{c}2} \\ -\rho S_{\mathrm{c}} V_{\mathrm{e}}^2 C_{L\mathrm{c}}\delta_{\mathrm{c}1} \\ \rho S_{\mathrm{c}} V_{\mathrm{e}}^2 \left[C_{D\mathrm{c}} \left(\delta_{\mathrm{c}1}^2 + \delta_{\mathrm{c}2}^2 \right) + C_{D\mathrm{c}0} \right] \end{bmatrix} \tag{12}$$

$$\boldsymbol{\tau}_{\mathrm{c}} = \begin{bmatrix} \rho S_{\mathrm{c}} V_{\mathrm{e}}^2 C_{L\mathrm{c}}\delta_{\mathrm{c}2} d_{\mathrm{c}} \\ \rho S_{\mathrm{c}} V_{\mathrm{e}}^2 C_{L\mathrm{c}}\delta_{\mathrm{c}1} d_{\mathrm{c}} \\ 0 \end{bmatrix} \tag{13}$$

where S_{c} is the effective lift area of one attitude control flap, $C_{D\mathrm{c}}$ is drag coefficient, $C_{D\mathrm{c}0}$ is zero lift drag coefficient, $\delta_{\mathrm{c}1}$ and $\delta_{\mathrm{c}2}$ are the angles of the deflections of the pitch control flaps and roll control flaps respectively, $C_{L\mathrm{c}}$ is lift coefficient, and d_{c} is the distance between the aerodynamic center of the control flap and the gravity center of the aerial vehicle.

Therefore, the aerodynamic forces and moments caused by the attitude control flaps of the small ducted fan aerial vehicle can be written as

$$\boldsymbol{f}_{\mathrm{flap}} = \boldsymbol{f}_{\mathrm{a}} + \boldsymbol{f}_{\mathrm{c}} = \begin{bmatrix} \rho S_{\mathrm{c}} V_{\mathrm{e}}^2 C_{L\mathrm{c}}\delta_{\mathrm{c}2} \\ -\rho S_{\mathrm{c}} V_{\mathrm{e}}^2 C_{L\mathrm{c}}\delta_{\mathrm{c}1} \\ f_1 + f_2 \end{bmatrix} \tag{14}$$

$$\boldsymbol{\tau}_{\mathrm{flap}} = \boldsymbol{\tau}_{\mathrm{a}} + \boldsymbol{\tau}_{\mathrm{c}} = \begin{bmatrix} \rho S_{\mathrm{c}} V_{\mathrm{e}}^2 C_{L\mathrm{c}}\delta_{\mathrm{c}2} d_{\mathrm{c}} \\ \rho S_{\mathrm{c}} V_{\mathrm{e}}^2 C_{L\mathrm{c}}\delta_{\mathrm{c}1} d_{\mathrm{c}} \\ -4\rho S_{\mathrm{a}} V_{\mathrm{e}}^2 (C_{L\mathrm{a}}\delta_{\mathrm{a}} + C_{L\mathrm{a}0}) d_{\mathrm{a}} \end{bmatrix} \tag{15}$$

where

$$\begin{cases} f_1 = 4\rho S_{\mathrm{a}} V_{\mathrm{e}}^2 \left(C_{D\mathrm{a}}\delta_{\mathrm{a}}^2 + C_{D\mathrm{a}0} \right) \\ f_2 = \rho S_{\mathrm{c}} V_{\mathrm{e}}^2 \left[C_{D\mathrm{c}} \left(\delta_{\mathrm{c}1}^2 + \delta_{\mathrm{c}2}^2 \right) + C_{D\mathrm{c}0} \right] \end{cases} \tag{16}$$

(4) Influence of the spinning moment

The high-speed spinning propeller provides the power for the small ducted fan aerial vehicle. When the attitudes of the vehicle change, the effect of the spinning moment will lead to the coupling phenomenon between the pitch channel and roll channel. The spinning moment can be expressed as

$$\boldsymbol{\tau}_{\mathrm{gero}} = [\, -I_{\mathrm{p}}\omega_{\mathrm{e}} q \quad I_{\mathrm{p}}\omega_{\mathrm{e}} p \quad 0 \,]^{\mathrm{T}} \tag{17}$$

where I_{p} is the inertia moment of the propeller with high-speed, ω_{e} is the angular rate of the propeller.

2.2.2. Parameter analysis and classification

In accordance with the features and attributes of the parameters, all parameters involved in the above equations are classified. The results of the classification are shown in Table 1.

The structural parameters mainly refer to the mass of the aerial vehicle, the rotational inertia and relative positions of the functional components. These parameters are basically confirmed during the design, and only need to be identified and corrected by experiments during the modeling. Aerodynamic parameters mainly include the aerodynamic coefficients related to the dynamic system, the reaction torque control flaps and the attitude control flaps. These parameters should be identified by experiment. Both motion parameters and controlling parameters are values involved during the actual flight tests, and can be obtained by using airborne sensors and recording devices.

3. Identification of structural and aerodynamic parameters

3.1. Identification of structural parameters

3.1.1. Mass and position parameters

The mass of an aerial vehicle refers to the total mass of all components, including the vehicle structure, the power equipment, the control system and the batteries. Component masses and the total mass of the ducted fan aerial vehicle studied by this paper are shown in Table 2.

Ducted fan aerial vehicles are axial symmetry systems. In this paper, the center position of the aerial vehicle is confirmed by a bifilar pendulum balance method and adjusted by adjusting the positions of the devices in the cabin. The origin of the coordinate frame of the ducted fan aerial vehicle is set at the position of the center of gravity.

In Fig. 2, the length of the arm of the reaction torque flap for the aerial vehicle equals the distance from the aerodynamic center to the axis O_bz_b of the coordinate frame of the airframe, denoted by d_a. The lengths of the arms of the pitching and rolling control-flaps equals the distances from the aerodynamic center to the axis O_by_b and axis O_bx_b respectively, denoted by d_c. Here d_a and d_c are design values, where $d_a = 0.08$ m, $d_c = 0.2$ m.

3.1.2. Rotational inertia

Ducted fan aerial vehicles are axial symmetry systems whose origins of the coordinate frame of the airframe are set at the position of the center of gravity. Its inertia moment is

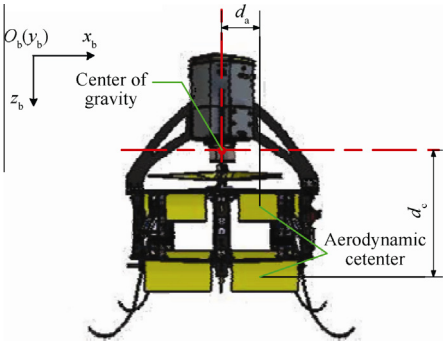

Fig. 2 Components and structure diagram.

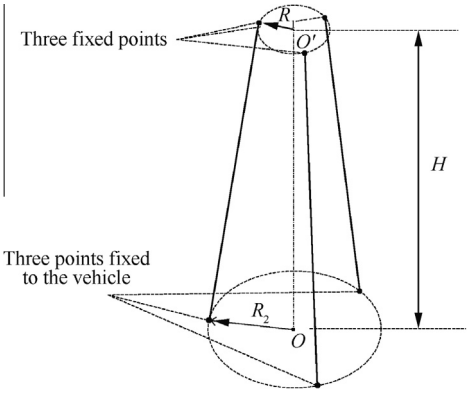

Fig. 3 Tri-wire pendulum method diagram.

Table 1 Parameters in mathematical model.

Parameter type	Parameters included	Evaluation method
Structure	m, I_x, I_y, I_z, I_p, d_c, d_a	Design and identification
Aerodynamic	K_f, K_t, C_{La}, C_{La0}, C_{Da}, C_{Da0}, C_{Lc}, C_{Dc}, C_{Dc0}	Identification
Motion	θ, ϕ, p, q, r, $\dot{p}$, $\dot{q}$, $\dot{r}$, u, v, w, $\dot{u}$, $\dot{v}$, $\dot{w}$	Flight measurement
Controlling	δ_e, δ_a, δ_{c1}, δ_{c2}	Controlled by input

Table 2 Mass distribution of systems.

System name	Content	Mass (kg)
Structure of the aerial vehicle	Airframe supporting the structure of the vehicle, undercarriage and other structures.	0.794
Flight control system	Attitude measurement unit, circuit board of the automatic pilot, connecting lines.	0.261
Attitude control system	Anti-torque flaps and pitching and rolling control flaps.	0.215
Dynamic system	Motor, propeller, electron speed regulator.	0.654
Airborne equipment	Cameras and wireless communication module.	0.122
Power source	Power batteries and cables.	0.764
Total mass	Total take-off mass.	2.81

Table 3 Experimental parameters.

Parameter	Value
Mass of the aerial vehicle m (kg)	2.81
Distance from the upper suspension point to the central axis R_1 (m)	0.12
Distance from the underside suspension point to the central axis R_2 (m)	0.18
Vertical distance of the suspension center H (m)	3.35

$I_{xy} = I_{xz} = I_{yz} = 0$. Therefore, the identification only involves the main diagonal of the inertial tensor. That is the identification of the rotational inertia. During the experiment, the tri-wire pendulum method is used to measure the rotational inertia of the rigid body. The tri-wire pendulum method diagram is shown in Fig. 3.[14]

According to the law of conservation of energy and the law of rotation of rigid body, the rotational inertia of the object rotating around the central axis OO'can be derived as follows:

$$I = \frac{mgR_2R_1}{4\pi^2 H} T_0^2 \tag{18}$$

where R_2 the distance from the underside suspension point to the central axis OO', R_1 the distance from the upper suspension point to the central axis OO', H the length of the suspension wire, T_0 the swing period. When the aerial vehicle takes the simple harmonic motion along OO' axis, the time for one complete cycle of any point in the aerial is defined as the swing period.

At the beginning of the experiment, the aerial vehicle is still, then it is rotated for 5° along the central axis OO', and the aerial vehicle is released to make a fixed-axis rotation around the central axis OO'. The rotation follows the law of simple harmonic motion. A stopwatch is used to record the time needed to accomplish 30 swing periods. The experiment is repeated for 5 times along each direction of the axes of the airframe, and all experimental data are recorded. The results in Table 3 can be obtained based on the above mentioned identification results and actual measurement.

The experimental data for rotational inertia I_z are shown in Table 4. The values of I_x and I_y can be obtained by the same method.

Table 4 Experimental data of I_z measurement.

Time	30 swing periods
1	79.7
2	79.3
3	80.1
4	79.0
5	79.6
Mean value	79.7

Table 5 Identification results.

Parameter	Value
Mass of the aerial vehicle m (kg)	2.81
Arm of the reaction torque flaps d_a (m)	0.08
Arm of controlling flaps d_c (m)	0.20
Rotational inertia of axis O_bx_b I_x (kg·m^2)	0.0391
Rotational inertia of axis O_by_b I_y (kg·m^2)	0.0391
Rotational inertia of axis O_bz_b I_z (kg·m^2)	0.0304

So far, we have completed the identification of the structural parameters. The identification results of the structural parameters are shown in Table 5.

3.2. Identification of aerodynamic parameters

3.2.1. Parameter identification related to rotor dynamics

The dynamic system of the ducted fan aerial vehicle mainly contains the motor, the propeller, the electronic speed regulator, and batteries. The thrust output of the dynamic system, the torque and the slip velocity caused by the propeller are given, respectively, by

$$\begin{cases} \boldsymbol{f}_r = \begin{bmatrix} 0 & 0 & -K_f n^2 \end{bmatrix}^T \\ \boldsymbol{\tau}_r = \begin{bmatrix} 0 & 0 & K_t n^2 \end{bmatrix}^T \\ V_e = K_v n \end{cases} \tag{19}$$

where K_v is the slip velocity coefficient of the dynamic system.

The parameters K_f, K_t and K_v are to be identified. Based on the sources and features of these parameters, a thrust and torque testing platform was designed for the ducted fan aerial vehicle.[15] The schematic diagram is shown as Fig. 4.

Hence, this testing system is composed of an active testing platform and a fixed platform as shown in Fig. 4. The active platform combines with the fixed one by the cylindrical linear guide rail. The measured motor and propeller are installed on the active platform. During the testing experiment, motor can make the propeller spin, and apply the pulling force and the torque to the active platform. At the same time, the pressure sensor and torque sensor can measure the pulling force and moment through the cylindrical linear guide rail. The galvanometer, the anemometer, and the tachometer are all behind the propeller, and it is convenient to test the current of the motor and measure the rotating speed and the sliding speed of the propeller timely. This testing system integrates many types of measuring sensors, including the pressure sensor, the torque sensor, the anemometer and the tachometer. The experimental apparatus for testing the dynamic system is shown in Fig. 5.

The data for the testing of the dynamic system are recorded in Table 6.

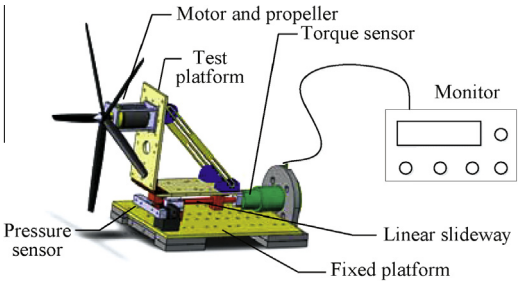

Fig. 4 Multiple-sensor testing platform.

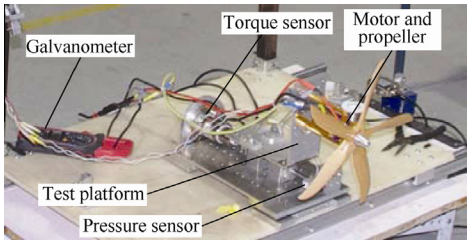

Fig. 5 Testing experiment of dynamic system.

Data fitting is conducted for the testing results. The fitting results are as follows:

(a) Data fitting result of the throttle control and the rotating speed

$$n = 1 \times 10^4 (e_t - 1.05)$$

where e_t is the time of high level for pulse width modulation (PWM) signal. Here, the motor is controlled by PWM signal.

(b) Data fitting result of the thrust and the rotating speed

$$F_b^z = 5.97 \times 10^{-8} n^2$$

i.e. the aerodynamic parameter is

$$K_f = 5.97 \times 10^{-8}$$

(c) Data fitting result of the torque and the rotating speed

$$\tau_b^z = 7.6 \times 10^{-9} n^2$$

i.e. the aerodynamic parameter is

$$K_t = 7.6 \times 10^{-9}$$

(d) Data fitting result of slip velocity and the rotating speed

$$V_e = 2.17 \times 10^{-3} n$$

where V_e is measured by the anemometer which is set behind the propeller, i.e. the aerodynamic parameter is

$$K_v = 2.17 \times 10^{-3}$$

3.2.2. Parameter identification for drag and lift

The attitude control flaps of the ducted fan aerial vehicle are located within the flow field of the wake flow caused by the propeller in the duct. Due to the ring effect of the duct, the features of the flow field within the duct are clearly different from that of an open flow field. Therefore, the parameters for traditional airfoil vehicles, such as the lift coefficient and the drag coefficient, are not applicable in this situation, and the parameter identification needs to be re-conducted.

(1) Conditions for aerodynamic parameter identification

This study adopts the method of finite element simulation to conduct a simulation analysis on the aerodynamic features of the duct control flaps. A momentum source with the same diameter as the propeller is used as the source of thrust, and the attitude control flaps of the simulation model are set the same as that of the practical model of the aerial vehicle in order to reflect accurately the aerodynamic features of the two layers of the attitude control flaps.[16] The simulation experimental results are presented in Fig. 6.

The main parameters of the simulation experiment and the parameter setting methods are as follows:

(a) The sizes of the reaction torque flaps and the pitching and rolling control flaps are preset in accordance with the originally designed value, $S_a = 0.0096\ m^2$ and $S_c = 0.01\ m^2$, respectively.
(b) In case of hovering and low-speed level flight, the value of thrust can be considered to be equal to the total mass of the aerial vehicle, that is 2.81 kg, and in this situation, the wind speed in the flow field within the duct is 16.7 m/s.

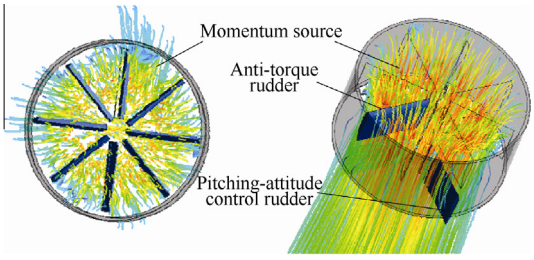

Fig. 6 Finite element simulation experiment of the attitude control flaps.

Table 6 Testing results of dynamic system.

Time (ms)	Rotating speed (r/min)	Thrust (N)	Torque (N•m)	Wind speed (m/s)
1.1	430	0.4	0.010	2.3
1.2	1438	2.1	0.025	4.7
1.3	2538	4.6	0.057	6.9
1.4	3559	8.2	0.105	9.1
1.5	4572	13.1	0.141	10.8
1.6	5642	18.3	0.215	13.4
1.7	6750	26.1	0.302	16.1
1.8	7590	33.2	0.391	18.1
1.9	8230	40.2	0.483	19.2

Table 7 Simulation experiments of attitude control flaps.

Deflection angle of the control flap	Forces of pitching and rolling control flaps (N)		Forces of reaction torque flaps (N)	
	Lift	Drag	Lift	Drag (10^{-2})
0°	0.017	0.121	0.216	0.306
2°	0.305	0.141	0.221	0.311
4°	0.583	0.161	0.219	0.308
6°	0.793	0.214	0.213	0.310
8°	1.155	0.249	0.226	0.313
10°	1.392	0.355	0.218	0.321

(c) The ideal working state of the reaction torque flap requires that when the angle of deflection equals 0°, the life can exactly overcome the spin torque of the dynamic system. The reaction torque flaps are symmetrically designed, and the force situations are all the same. Experiments will be carried out to examine the force situation of only one of the flaps.

(d) The pitching and rolling control flaps are symmetric airfoils. Their lift and drag have nothing to do with the direction but with the angle of the deflection of the flaps. Experiments will be carried out to analyze the force situations of one pitching and rolling flap at the angle of the deflection at 0°, 2°, 4°, 6°, 8°, 10°.

Data of the simulation experiments are shown in Table 7.

(2) Identification results of the aerodynamic parameters of the reaction torque flaps

As indicated in paragraph (c), the ideal angle of deflection of the reaction torque flaps is 0°. In this circumstance, the lift on the control surface is expected to exactly overcome the spin torque of the dynamic system of the aerial vehicle. After carrying out testing on the dynamic system of the aerial vehicle, it can be found that the lift L_a provided equals 0.219 N, and the drag D_a equals 0.312 N. The equations of the aerodynamic lift and drag provided by the reaction torque flaps are given, respectively, by

$$\begin{cases} L_a = \frac{1}{2}\rho S_a V_e^2 (C_{La}\delta_a + C_{La0}) \\ D_a = \frac{1}{2}\rho S_a V_e^2 (C_{Da}\delta_a + C_{Da0}) \end{cases} \tag{20}$$

where the parameter values are as follows: $\rho = 1.205\ \mathrm{kg/m^2}$, $S_a = 0.0096\mathrm{m}^2$, and $V_e = 16.7$ m/s.

Substitute all parameter values into the lift and drag calculating Eq. (20) to find that

$$\begin{cases} 0.219 = \frac{1}{2} \times 1.205 \times 0.0096 \times 16.7^2 C_{La0} \\ 0.312 = \frac{1}{2} \times 1.205 \times 0.0096 \times 16.7^2 C_{Da0} \end{cases}$$

Solve the above equation to get the lift coefficient and the drag coefficient when the angle of deflection of the reaction torque flaps is zero. The results are as follows:

$$C_{La0} = 0.1358, C_{Da0} = 0.0323$$

(3) Identification results for the aerodynamic parameters of the pitching and rolling control flaps

The airfoil profiles and sizes of the four pitching and rolling flaps are the same. During the simulation experiments, we only need to examine the force situation of one control flap. The aerodynamic lift on the surface of the control flap can be obtained by using the finite element simulation method. Data fitting for the aerodynamic lift leads to

$$L_c = 0.1432\delta_c + 0.0005 \tag{21}$$

Therefore, the expression of the aerodynamic lift of the control flap is as follows:

$$L_c = \frac{1}{2}\rho S_c V_e^2 C_{Lc}\delta_c \tag{22}$$

in which,

$$\begin{cases} \rho = 1.205\ \mathrm{kg/m^2} \\ S_c = 0.01\ \mathrm{m^2} \\ V_e = 16.7\ \mathrm{m/s} \end{cases}$$

Join the data fitting Eq. (21) with the lift Eq. (22) to get

$$\frac{1}{2}\rho S_c V_e^2 C_{Lc}\delta_c = 0.1432\delta_c$$

That is to say:

$$C_{Lc} = 8.5 \times 10^{-2}$$

By the same procedure, coefficients related to drag can be calculated:

$$C_{Dc} = 1.3 \times 10^{-3}$$

$$C_{Dc0} = 7.47 \times 10^{-2}$$

So far, the identification of aerodynamic parameters has basically been completed. The identification results of the aerodynamic parameters are presented in Table 8.

3.2.3. Dynamic model discussion

(1) Overall dynamic equation

The above parameters are substituted into the dynamics Eq. (5) to obtain the following flight dynamics model for single-blade ducted aerial vehicles:

$$\begin{bmatrix} -mg\sin\theta + \rho S_c V_e^2 C_{Lc}\delta_{c2} \\ mg\cos\theta\sin\phi - \rho S_c V_e^2 C_{Lc}\delta_{c1} \\ mg\cos\theta\cos\phi - K_f n^2 + 4\rho S_a V_e^2 (C_{Da}\delta_a^2 + C_{Da0}) + \\ \rho S_c V_e^2 [C_{Dc}(\delta_{c1}^2 + \delta_{c2}^2) + C_{Dc0}] \end{bmatrix} = \begin{bmatrix} m(\dot{u} + qw - rv) \\ m(\dot{v} + ru - pw) \\ m(\dot{w} + pv - qu) \end{bmatrix} \tag{23}$$

Table 8 Identification results.

Parameter	Value
Thrust coefficient of the propeller K_f	5.97×10^{-8}
Torque coefficient of the propeller K_t	7.6×10^{-9}
Coefficient of the slip velocity K_v	2.7×10^{-3}
Lift coefficient of the anti-torque flap at 0° deflection C_{La0}	1.358×10^{-1}
Drag coefficient of the anti-torque flap at 0° deflection C_{Da0}	3.23×10^{-2}
Lift coefficient of the control flap C_{Lc}	8.5×10^{-2}
Drag coefficient of the control flap C_{Dc}	1.3×10^{-3}
Drag coefficient of the control flap at 0° deflection C_{Dc0}	7.47×10^{-2}

$$\begin{bmatrix} \rho S_c V_e^2 C_{Lc}\delta_{c2} d_c - I_p\omega_e q \\ \rho S_c V_e^2 C_{Lc}\delta_{c1} d_c + I_p\omega_e p \\ K_t n^2 - 4\rho S_a V_e^2 (C_{La}\delta_a + C_{La0}) d_a \end{bmatrix} = \begin{bmatrix} I_x\dot{p} + qr(I_z - I_y) \\ I_y\dot{q} + rp(I_x - I_z) \\ I_z\dot{r} + pq(I_y - I_x) \end{bmatrix} \tag{24}$$

(2) Attitude control model

The paper is mainly about the attitude model of the ducted fan aerial vehicle, and gives the relevant designs of the control flaps. The dynamic equations of the pitch and roll attitude loop are as

$$\begin{cases} L = I_x\dot{p} + qr(I_z - I_y) \\ M = I_y\dot{q} + rp(I_x - I_z) \end{cases} \tag{25}$$

According to Eq. (24), the corresponding aerodynamic moments can be derived as

$$\begin{cases} L = \rho S_c V_e^2 C_{Lc}\delta_{c2} d_c - I_p\omega_e q \\ M = \rho S_c V_e^2 C_{Lc}\delta_{c1} d_c + I_p\omega_e p \end{cases} \tag{26}$$

In applying the assumption of the small-disturbance theory, Eq. (25) can be simplified:

$$\begin{cases} \Delta L = \dfrac{\partial L}{\partial n}\Delta n + \dfrac{\partial L}{\partial \delta_{c2}}\Delta\delta_{c2} + \dfrac{\partial L}{\partial q}\Delta q \\ \Delta M = \dfrac{\partial M}{\partial n}\Delta n + \dfrac{\partial M}{\partial \delta_{c1}}\Delta\delta_{c1} + \dfrac{\partial L}{\partial p}\Delta p \end{cases} \tag{27}$$

where ΔL and ΔM are changes of rolling moment and pitching moment; Δp and Δq are state variables, denoting the angular rates of the pitching and rolling of the aerial vehicle respectively, $\Delta\delta_{c1}$ and $\Delta\delta_{c2}$ are control variables, denoting the angles of deflection of the control flaps in the pitching and rolling directions; and Δn is the change of propeller speed.

Substitute the results of the identified parameters into Eq. (27), we can get

$$\begin{cases} \dfrac{\partial L}{\partial n} = \dfrac{\partial M}{\partial n} = 0 \\ \dfrac{\partial L}{\partial \delta_{c2}} = \dfrac{\partial M}{\partial \delta_{c1}} = 12.05 d_c S_c \\ \dfrac{\partial L}{\partial q} = \dfrac{\partial M}{\partial p} = 2.36 \end{cases} \tag{28}$$

Thus, the dynamic equations of the attitude control loop can be obtained as

$$\begin{cases} 2.41 S_c\Delta\delta_{c2} + 2.36\Delta q = I_x\Delta\dot{p} \\ 2.41 S_c\Delta\delta_{c1} + 2.36\Delta p = I_y\Delta\dot{q} \end{cases} \tag{29}$$

Based on Eq. (29), what the paper researched next is about the design of the control flaps.

4. Completion of the design for the control flaps using the model obtained based on the identification

4.1. Design for control flaps

The effective lift surface area S_c and the length of the arm of the acting force d_c of the control flaps need to be confirmed. These are also the design variables of the design of the control flaps. The structural and aerodynamic parameters obtained in Section 3 are substituted into Eq. (29), the flight dynamics model of the aerial vehicle in Section 2, and then the method of small disturbance and linearization is used to obtain the following state space expression of the ducted aerial vehicle:

$$\begin{bmatrix} \Delta\dot{p} \\ \Delta\dot{q} \end{bmatrix} = \begin{bmatrix} 0 & 1.05 \\ 1.05 & 0 \end{bmatrix}\begin{bmatrix} \Delta p \\ \Delta q \end{bmatrix} + \begin{bmatrix} 0 & 308.18 d_c S_c \\ 308.18 d_c S_c & 0 \end{bmatrix}\begin{bmatrix} \Delta\delta_{c1} \\ \Delta\delta_{c2} \end{bmatrix} \tag{30}$$

where Δp and Δq are system state variables, denoting, respectively, the angular velocities of the pitching and rolling of the aerial vehicle. $\Delta\delta c_1$ and $\Delta\delta c_2$ are controlled by the system, denoting the angles of deflection of the control flaps in the pitching and rolling directions.

According to the actual flight data of the aerial vehicle, the aerial vehicle will be disturbed by the external environmental conditions, such as a crosswind. The disturbance quantity will cause the airframe of the ducted aerial vehicle to have an angular velocity of about 10 (°)/s. In this circumstance, assume that the control flaps of the aerial vehicle have reached their maximum controlling-position for controlling the vehicle. The state variables $\Delta p = \Delta q = 12$ (°)/s and the control variables $\Delta\delta_{c1} = \Delta\delta_{c2} = 12°$ are substituted into Eq. (30), which are obtained by flight tests. Then, the conditional expression of the controllability of the aerial vehicle is resolved to find that

$$\Delta\dot{p} = \Delta\dot{q} = 10.5 - 3698.16 d_c S_c < 0$$

That is to say,

$$d_c S_c > 0.0028$$

A larger value for d_c indicates a closer distance to the bottom of the duct. For convenience when conducting the process and the experiment, it is best to make d_c as large as possible. Additionally, the increase of d_c will enlarge the space for the value design of aerodynamic chord of control flap. Therefore, in this paper, the value of d_c is set as 0.25 m, and thus the lift area of the control flap S_c is larger than 0.0144 m^2.

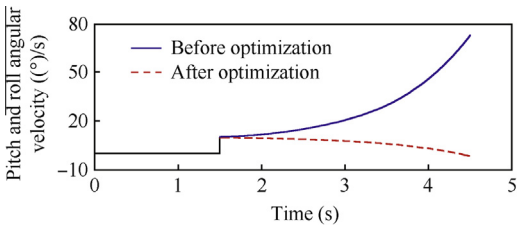

Fig. 7 Simulation of restoring tendency after disturbing aerial vehicle.

4.2. Simulation verification of the results of the pitching and rolling control flaps

The condition set for the simulation experiment is that, when $t = 1.5$s, the system is supplied with a certain quantity of disturbance to produce an angular velocity of $\Delta p = \Delta q = 10$ (°)/s. Meanwhile, the control flap must make sure to reach the maximum position in the opposite direction. That is, the controlled quantity $\Delta\delta_{c1} = \Delta\delta_{c2} = -12°$. The motion states of the model before and after parameter optimization are shown in Fig. 7.

According to the simulation diagram, with respect to the model of the aerial vehicle before the optimization, even when the control flap reaches the maximum steerage, it is still impossible to prevent the aerial vehicle from deviating from the equilibrium position, and as time elapses, the instability phenomenon of the aerial vehicle becomes more and more significant. After parameter optimization, when the control flap reaches the maximum steerage, the aerial vehicle shows a tendency towards a stable state, and as time elapses, such a tendency becomes more and more significant. Therefore, it improves the aerial vehicle's capacity to resist disturbance from the architectural perspective.

4.3. Flight test verification

Flight tests, shown in Fig. 8, are carried out to observe and verify the overall effect after the optimization of the attitude control units.

State parameters of the aerial vehicle are sent back using a wireless module to carry out an off-line analysis. The changes for one flight are shown in Fig. 9.

According to Fig. 9, the aerial vehicle is able to return to the stable state gradually when it is disturbed by the external environment. It means that the design of the control structures of the aerial vehicle can significantly improve the controllability of the aerial vehicle.

(a) Outdoor (b) Indoor

Fig. 8 Outdoor and indoor flight tests of the ducted fan aerial vehicle.

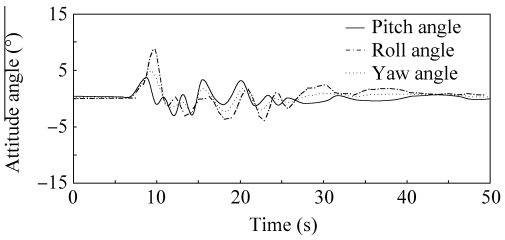

Fig. 9 Flight attitude situation during the flight verification experiment.

5. Conclusions

(1) A method that dynamically integrates the structural design and the control system design of the ducted aerial vehicle is provided. The aerial vehicle architecture is carried out based on the requirements of the structural parameters using the control system of the aerial vehicle.

(2) A mathematical model with better controllability using proper structural design is obtained. Through the flight test, the accuracy of modeling and identification processes for this small aerial vehicle is verified.

Acknowledgement

This study was supported by the National Natural Science Foundation of China (No. 11102019).

References

1. Cycon JP, Hunter DH, Krauss TA. Snubber assembly for a rotor assembly having ducted, coaxial counter-rotating rotors. Hartford, CT: United Technologies Corporation; United States Patent US5340279; 1994.
2. Graf WE. *Effects of duct lip shaping and various control devices on the hover and forward flight performance of ducted fan UAVs* [dissertation. Blacksburg, VA: Virginia Polytechnic Institute and State University; 2005.
3. Metni N, Pflimlin JM, Hamel T, Soueres P. Attitude and gyro bias estimation for a flying UAV. In: *IEEE/RSJ International Conference on Intelligent Robots and Systems*; 2005. p.1114–20.
4. Ohanian OJ, Karni ED, Londenberg WK, Gelhausen PA, Inman DJ. Ducted-fan and moment control via steady and synthetic jets. *J Aircraft* 2011;**48**(2):514–26.
5. Pflimlin JM, Soueres P, Hamel T. Waypoint navigation control of a VTOL UAV amidst obstacles. In: *IEEE/RSJ International Conference on Intelligent Robots and Systems*, 2006 Oct 9–15; Bejing, China; 2006. p. 3544–9.
6. Fantail VTOL miniature UAV [Internet]. Singapore: Singapore Technologies Aerospace (ST Aero); 2006 July 26 [cited 2011 Nov 18]. Available from: http://defense-update.com/products/f/fantail.htm.
7. Marconi L, Naldi R, Sala A. Modeling and analysis of a reduced-complexity ducted MAV. In: *14th Mediterranean Conference on Control and Automation 2006*; 2006. p. 1–5.
8. Naldi R, Marconi L, Sala A. Modelling and control of a miniature ducted-fan in fast forward flight. In: *American Control Conference*, 2008 June 11–13; Seattle, WA, USA; 2008. p. 2552–7.

9. Ko A, Ohanian JO, Gelhausen P. Ducted fan UAV modeling and simulation in preliminary design; 2007. Report No.: AIAA-2007-6375.
10. Akturk A, Camci C. Influence of tip clearance and inlet flow distortion on ducted fan performance in VTOL UAVs [Internet]. Available from: http://www.personal.psu.edu/faculty/c/x/cxc11/papers/AHS_2010_Forum66_AA_CC.pdf.
11. Akturk A, Camci C. A computational and experimental analysis of a ducted fan used in VTOL UAV systems [Internet]. 2011 Feb 23[cited 2011 Nov 18]. Available from: http://www.personal.psu.edu/cxc11/publications.html.
12. Anderson JD. *Fundamentals of aerodynamics*. 4th ed. New York: McGraw-Hill; 2005.
13. Sudani N, Kanda H, Sato M, Hitoshi M, Kenichi M, Susumu T. *Evaluation of NACA0012 airfoil test results in the NAL two-dimensional transonic wind tunnel*. 1st ed. Tokyo: National Aerospace Laboratory; 1991.
14. Song Ch, Pan J, Ye Y, Zhuang B. Measuring moment of inertia using tri-linear pendulum and its experimental error. *J Mech Pract* 2003;**1**:13–5 [Chinese].
15. Wang ZJ, Guo SJ, Li Ch. Numerical analysis of aerodynamic characteristics for the design of a small ducted fan aircraft. *Proc Inst Mech Eng Part G: J Aerosp Eng* 2013;**227**(10):1571–82.
16. Veldhuis LLM, Nebiolo S. Analysis of calculated and measured wake characteristics of a propeller-wing model; 2000. Report No.: AIAA-2000-0908.

Wang Zhengjie is an associate professor and Ph.D. supervisor at School of Mechatronical Engineering, Beijing Institute of Technology, Beijing, China. She received the Ph.D. degree from the same university in 2001. Her current research interests are small aircraft design and guidance and control for UAV.